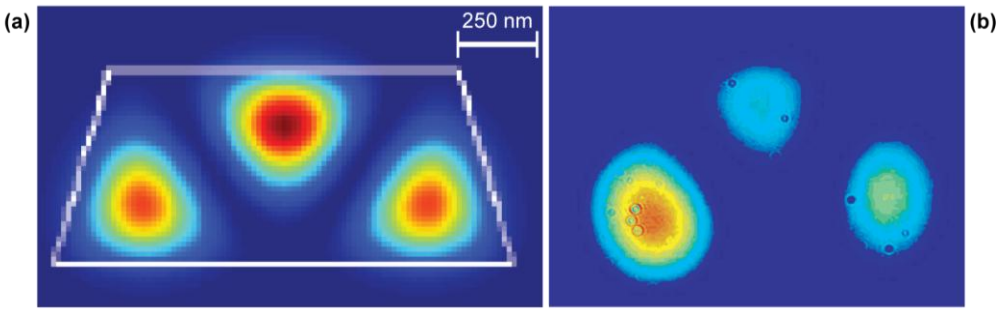

Fig. 3. Modal cross-section profiles for phase-mathched SH generation. (a) The simulated cross-section mode profile for the sixth-order mode of our waveguide at 777.1 nm. (b) The captured mode image of the visible emission from our waveguide showing good agreement with the simulated mode profile.

3.3 Third-harmonic generation

In addition to SH, we also observe third-harmonic generation in the ring resonators as shown in Fig. 4(a). The intrinsic $\chi^{(3)}$ nonlinearity of the silicon nitride induces the third order process in which three pump photons generate a single photon at the third-harmonic frequency. Efficient THG requires meeting the same phase-matching condition as SHG: the effective index of the pump must equal the effective index at the TH wavelength. By performing similar simulations as before we find the fundamental mode of the pump is closest in refractive index to the 18th order mode at the third-harmonic wavelength.

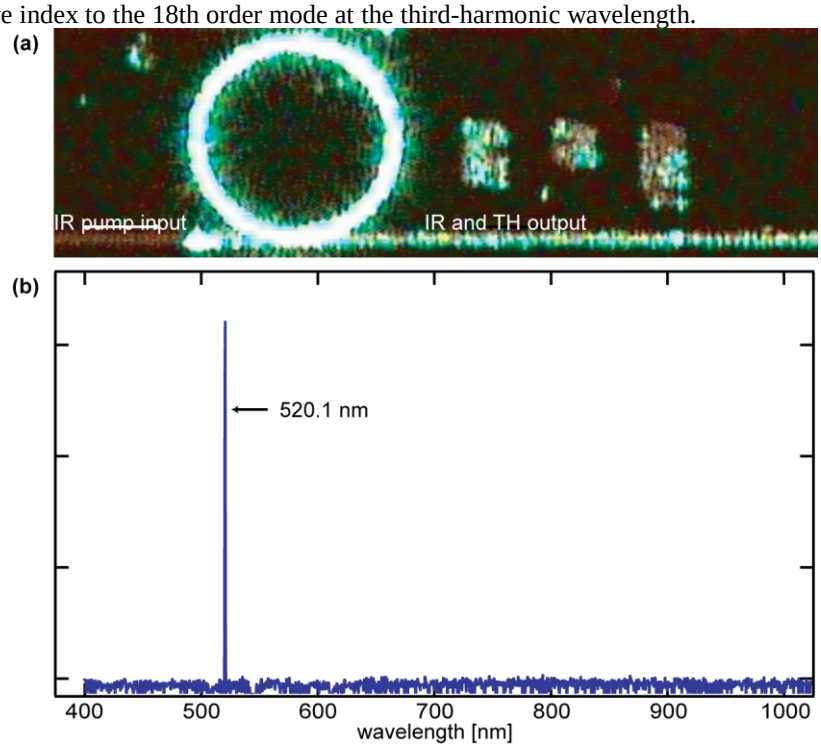

Fig. 4. Third-harmonic generation in silicon nitride resonators. (a) Top view CCD image of waveguide coupled ring resonator generating visible TH from an IR pump tuned to the cavity resonance. (b) Spectrometer output from the waveguide shown in (a). The monochromatic response confirms the wavelength and that THG is occurring.

By pumping at a resonance near 1560 nm, we generate the TH and measure the light to be exactly one third of the pump wavelength (Fig. 4). We are able to measure picowatts of output power with for the same pump strength as used to generate SH light. This is on the same order

#146538 - $15.00USD Received 28 Apr 2011; revised 22 May 2011; accepted 23 May 2011; published 26 May 2011

as shown in a silicon photonic crystal [2], but here light is coupled and guided in the bus waveguide as opposed to out of plane emission.

4. Analysis

We calculate the effective $\chi^{(2)}$ to be as large as 4 x 10^{-14} m/V from the conversion efficiency observed in the ring. For SHG with an undepleted pump, the expected signal power may be calculated for a given pump intensity and propagation distance by solving the coupled amplitude equations [22]. Since we are using a resonator, the intensity of the pump and SH are increased by the respective cavity enhancement effects of the ring. In order to accurately model the nonlinear susceptibility, we take into account the finesse of the cavity, the simulated modal field overlap and phase-mismatch, and the radius of the ring. The power P_{sh} for second harmonic wave is then given by:

$$P_{sh} = \frac{C_{sh}C_p^2(\omega_p \chi^{(2)} L P_p)^2}{8n_p^2 n_{sh} c^3 \epsilon_0 A_p^2} A_{sh} \sin c^2(\Delta k L/2)\ f(A_p, A_{sh}),$$
$$C_i = \frac{P_{circ}}{P_{in}} = \left| \frac{j\kappa_i \exp(-\alpha_i L/2)}{\exp(jk_i L) - \tau_i \exp(-\alpha_i L/2)} \right|^2 \quad (1)$$

where ω_p is the pump frequency, ε_0 is the permittivity of free space, c is the speed of light in vacuum, n_i is the effective index for the modes, A_i is the mode area, Δk is the phase mismatch, L is the ring circumference and P_p is the pump power in the waveguide. The modal overlap integral between the fundamental and second-harmonic fields is accounted for by the function $f(A_p,A_{sh})$. C_i takes into account the circulating power in the ring [15] where κ and τ represent the coupling parameters from the waveguide to the ring, α is the propagation loss in the ring and k_i is the wavenumber. We can directly measure C_p from the transmission spectrum of the pump resonance and calculate this to be approximately 156. For the SH resonance we are unable to directly characterize the intrinsic and coupling Q's. We estimate that C_{sh} is at most C_p and at least unity. From this approximation we come up with a range of potential values for the effective $\chi^{(2)}$ 3 x 10^{-15} to 4 x 10^{-14} m/V. We believe the actual enhancement at the SH wavelength is closer to unity than C_p and therefore the effective $\chi^{(2)}$ to be on the larger side of the approximation range. From Eq. (1), we see that the SH wave has a quadratic dependence on the pump power and nonlinear susceptibility $\chi^{(2)}$. In order to clearly demonstrate the theoretical square dependence of the SH process, we plot the dropped pump power against the generated SH on a log-log scale (Fig. 5) and calculate a best fit slope of 1.9745 ± 0.0225. From the measured output power values we estimate our induced $\chi^{(2)}$. The integrated high finesse resonator in silicon nitride increases the efficiency of the SHG significantly when the pump and SH are both resonant.

#146538 - $15.00 USD Received 28 Apr 2011; revised 22 May 2011; accepted 23 May 2011; published 26 May 2011

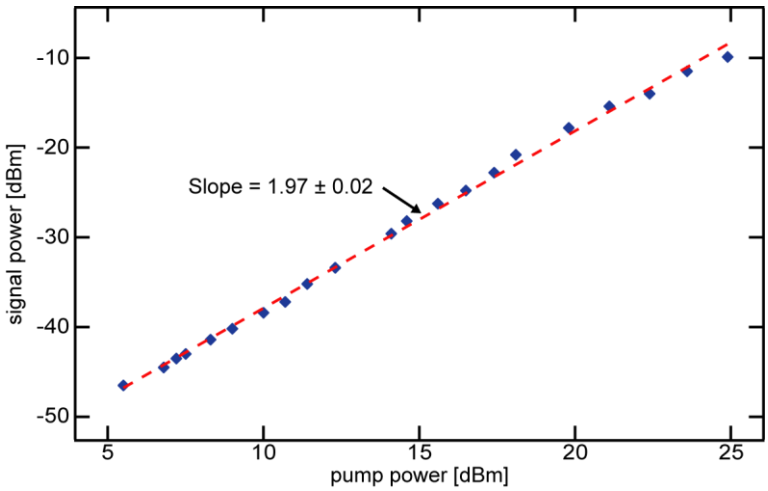

Fig. 5. The power dependence of generated SH coupled out versus pump power dropped to the ring. The red-dashed line with slope near 2 on the log-log plot represents the best fit line of the experimental data and is very close to the theoretical square prediction.

The $\chi^{(3)}$ response in silicon nitride has been previously examined [5–7] by quantifying the nonlinear refractive index, n_2, through the Kerr-shift, self-phase modulation and four-wave mixing respectively. Like previous work involving SiO_2 resonators [4], we expect to see THG with high enough circulating powers and phase-matching to higher order modes from the bulk nonlinearity as opposed to an enhanced surface effect with the SHG. From the spectrometer measurements taken to confirm the wavelength of the harmonic, we can measure the collected photons over a specified integration time. From this data we calculate the collected power to be on the order of picowatts with a maximum input power of 120 mW dropped into the ring. Given the circulating power in the resonator, the nonlinearity of the material and the cubic dependence of the third-harmonic power on the pump intensity, we expect much stronger conversion efficiencies. We believe that imperfect phase-matching and the weak spatial overlap between the fundamental and third-harmonic modes may account for the weaker than expected third harmonic. Therefore, our estimation of the effective $\chi^{(2)}$ could be a lower bound since we assume ideal phase-matching, as suggested by our simulations, in this approximation.

5. Conclusions

Our demonstration of guided on-chip visible light generation opens the available spectrum for Si-based devices from the IR to the visible, increasing bandwidth and enabling potential integration of silicon photodetectors to on-chip optical networks. We have demonstrated an integrated coupling of both the second and third harmonics from a cavity to a waveguide for the first time on a silicon platform. Additionally, the doubly resonant SH generation presented here could produce squeezed states [23] of both the pump and SH frequencies for quantum optics studies. Finally, the induced second-order nonlinearity could be used for difference frequency generation to combine two near infrared pumps to generate a mid-infrared source [24].

Acknowledgements

The authors would like to acknowledge DARPA for supporting this work under the MTO POPS Program. This work was performed in part at the Cornell NanoScale Facility, a member of the National Nanotechnology Infrastructure Network, which is supported by the National Science Foundation (Grant ECS-0335765).

#146538 - $15.00 USD Received 28 Apr 2011; revised 22 May 2011; accepted 23 May 2011; published 26 May 2011